First-principles study of the electronic and vibrational properties of $LiNbO_2$

Erik R. Ylvisaker and Warren E. Pickett
Department of Physics, University of California, Davis, California 95616, USA
(Received 14 February 2006; published 15 August 2006)

In the layered transition metal oxide $LiNbO_2$ the Nb^{3+} ($4d^2$) ion is trigonal-prismatically coordinated with O ions, with the resulting crystal field leading to a single band system for low energy properties. A tight-binding representation shows that intraplanar second neighbor hopping $t_2=100$ meV dominates the first neighbor interaction ($t_1=64$ meV). The first and third neighbor couplings are strongly modified by oxygen displacements of the symmetric Raman-active vibrational mode, and electron-phonon coupling to this motion may provide the coupling mechanism for superconductivity in Li-deficient samples (where $T_c \approx 5$ K). We calculate all zone-center phonon modes, identify infrared (IR) and Raman active modes, and report LO-TO splitting of the IR modes. The Born effective charges for the metal ions are found to have considerable anisotropy reflecting the degree to which the ions participate in interlayer coupling and covalent bonding. Insight into the microscopic origin of the valence band density, composed of Nb d_{z^2} states with some mixing of O $2p$ states, is obtained from examining Wannier functions for these bands.

DOI: 10.1103/PhysRevB.74.075104 PACS number(s): 71.20.−b, 71.20.Nr, 71.23.An, 74.70.Dd

I. INTRODUCTION

The quasi-two-dimensional (2D) compound $LiNbO_2$ has become of interest in condensed matter studies in no small part due to the existence of superconductivity[1] in the delithiated phase Li_xNbO_2. This system consists of a triangular lattice of transition metal (niobium) ions separated by layers of O ions from blocking (Li) layers, thus possessing structural similarities to high temperature superconducting cuprates. Important differences from the cuprates include the presence of a $4d$ rather than $3d$ ion, and of course the triangular rather than square lattice. The trigonal prismatic coordination of Nb with six O atoms causes the valence band to be composed solely of Nb d_{z^2} states. Other d states are well separated by a 2 eV gap, leaving only a single band per formula unit required for analysis. The comparative structural simplicity of $LiNbO_2$ makes it attractive for theoretical studies, especially as it requires modest computational time to characterize its properties.

This alkaliniobate is also of interest due to the increasing attention garnered by niobates in recent years.[2] The three-dimensional $LiNbO_3$ is an important and well studied ferroelectric material.[3] Superconductivity at $T_c \sim 20$ K has been reported by a few groups[4–6] in the barium niobate system. The phase has not been positively identified but it has been suggested to be a nonstoichiometric $BaNbO_x$ cubic perovskite. Superconductivity in the 5–6 K range has been reported in the Li-intercalated layered perovskite system $Li_xAB_2Na_{n-3}Nb_nO_{3n+1}$ (A=K,Rb,Cs; B=Ca,Sr,Ba; n=3 and 4).[7,8] This system has clear structural motifs in common with the peculiar $Nb_{12}O_{29}$ system, where the single O^{2-} deficiency (with respect to insulating $Nb_2O_5=Nb_{12}O_{30}$) releases two carriers into the cell; one localizes and is magnetic while the other is itinerant and results in conducting behavior.[9,10]

While there is good agreement as to structure type and lattice parameters of the stoichiometric phase $LiNbO_2$, there is some disagreement in the literature as to its electronic and magnetic properties. Originally it was reported as being paramagnetic with strong field dependence,[11] however calculations predict it to be a diamagnetic semiconductor.[12] Other experimental work suggests that it is diamagnetic, and strongly field-dependent paramagnetic properties are the result of impurities.[13] The values of the band gap are also in mild dispute. Extended Hückel calculations with a single isolated NbO_2 layer give a band gap value of 1.4 eV,[12] and full potential linear muffin tin orbital calculations with the full crystal structure of $LiNbO_2$ give 1.5 eV.[14] Measured optical reflectance shows an onset at ~2 eV, which is suggested to be a direct band gap responsible for the burgundy-red color of $LiNbO_2$.[13] Band structure calculations given here and by Novikov *et al.*[14] are in agreement that $LiNbO_2$ is a direct gap semiconductor.

Geselbracht, Richardson and Stacy[1] first reported that the delithiated phases Li_xNbO_2 with $x=0.45$ and $x=0.50$ support superconductivity at temperatures below 5.5 K and 5 K, respectively. Moshopoulou, Bordet, and Capponi[15] later reported samples with x ranging from 0.69 to 0.79 showing the onset of the Meissner effect at 5.5 K, but samples with $x=0.84$ and above do not exhibit any superconducting transition down to 2 K. Superconductivity has also been reported in hydrogen-inserted H_xLiNbO_2, in which both samples reported had the same $T_c=5.5$ K for $x=0.3$ and $x=0.5$.[16]

Removal of Li has the effect of adding holes to the conduction band made up of Nb d_{z^2} states. As mentioned above, there does not appear to be any notable dependence[1,15] of T_c on the concentration of Li in the range $0.45<x<0.8$. Such concentration independence has also been observed in the 2D electron-doped system[17,18] Li_xZrNCl. For a phonon-paired superconductor with cylindrical Fermi surfaces this behavior is understood in terms of phase space restrictions on phonon scattering processes[19] in 2D. The independence of T_c on carrier concentration in this system is quite surprising however, since the density of states (DOS) plots presented by Novikov *et al.*[14] and here varies strongly with energy, whereas parabolic bands lead to a constant DOS in 2D. There has also been some work done investigating the ion mobility of $LiNbO_2$ to assess its potential usefulness as a battery material.[13,20]

In this work we study the electronic structure and bonding of stoichiometric $LiNbO_2$ using density functional theory in the local density approximation (LDA). Density functional perturbation theory is used to obtain zone center phonons and Born effective charges. The structure contains a single parameter z that specifies the position of the O layers relative to the Li and Nb layers, and which seems to be of particular importance in understanding the electronic bonding and electron-phonon coupling in this compound. We investigate the corresponding Raman active vibrational mode (beating oscillation of the O planes) and the effect this has on the band structure. We obtain a tight-binding (TB) model that requires many neighbors and helps one to understand how this variation affects interactions between the Nb atoms. Many aspects of the electronic structure, such as chemical bonding and effective charges, can be seen to be interrelated by examining the Wannier functions of the valence bands.

II. STRUCTURE

Structural information of $LiNbO_2$ has been reported by several experimental groups, leading to the assignment of space group $P6_3/mmc$ (No. 194), with Li occupying sites $2a$ (0,0,0) with symmetry $\bar{3}m$, Nb occupying sites $2d$ $(\frac{2}{3},\frac{1}{3},\frac{1}{4})$ with symmetry $\bar{6}m2$, and O occupying sites $4f$ $(\frac{1}{3},\frac{2}{3},z)$ with symmetry $3m$. The O sites include an internal parameter z specifying their height relative to the Li layer along the c axis. The Li sites are centers of inversion; the Nb sites have z-reflection symmetry in addition to the $3m$ triangular symmetry within the layer but do not lie at centers of inversion.

There is good experimental agreement on lattice parameters, $a=2.90$ Å, $c=10.46$ Å.[11,13,15] The distance a between Nb atoms is quite close to the nearest neighbor distance of 2.86 Å in elemental bcc Nb, suggesting that direct Nb-Nb coupling should be kept in mind. However, $Nb^{3+}4d$ orbitals will be smaller than in neutral Nb. In later sections, we will discuss details of the Nb-O interactions, and show that the electronic properties of $LiNbO_2$ are very sensitive to changes in the Nb-O distance. The vertical distance between Nb and O planes can be calculated by $(\frac{1}{4}-z)c$, and the distance between Nb and O atoms is given by $\sqrt{\frac{2}{9}a^2+(\frac{1}{4}-z)^2c^2}$.

Some disagreement exists about the value of z. A larger value of z indicates the O layers are closer to the Nb layers. Meyer and Hoppe[11] found $z=0.1263$, Moshopoulou, Bordet, and Capponi[15] report $z=0.128$, Geselbracht *et al.*[13] report $z=0.124\,78$, Tyutyunnik *et al.*[21] report $z=0.1293$. These variations amount to a difference in O layer position of about 0.05 Å.

Optimization of unit cell geometry within LDA leads to $a=2.847$ Å, $c=10.193$ Å, $z=0.1211$. This differs from the measured value by $\Delta a\approx -1.8\%$, $\Delta c\approx -2.5\%$, for a total volume discrepancy of $\Delta V/V\approx -6\%$. The calculated overbinding of the unit cell is somewhat larger than is typical in LDA calculations, perhaps due to the low (practically zero) valence electron density in the Li layer. In this regard, we note that our Nb pseudopotential does not include the $4p$ states in the valence bands, which may have some effect on structural properties. Optimization with respect to z, holding the lattice parameters a and c fixed at experimental values gives $z=0.125$, which is very close to the value of Geselbracht *et al.*[13]

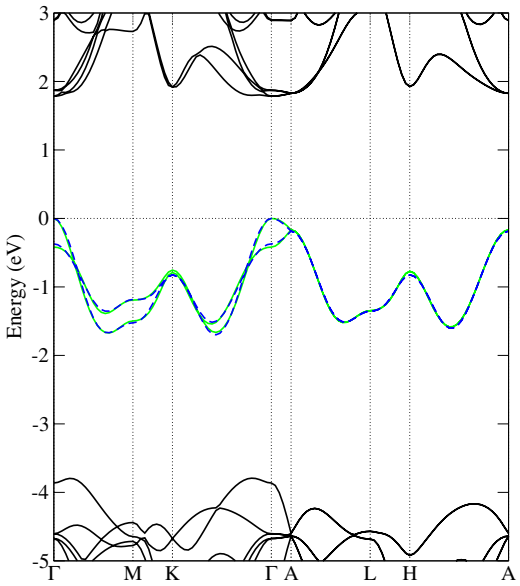

FIG. 1. (Color online) Band structure for $LiNbO_2$ with O height $z=0.1263$ typical of the slightly scattered experimental results. Two Nb bands (one per Nb layer) lie within a 5.5 eV gap between the O $2p$ bands below and the remaining Nb $4d$ bands above. The tight binding fit of Table I is shown with a dashed line.

III. ELECTRONIC STRUCTURE CALCULATIONS

The present results have been obtained through the use of the ABINIT code.[22] The lattice constants and the parameter z given by Meyer and Hoppe[11] were used in the calculations in this section. Pseudopotentials used were LDA, Troullier-Martins type,[23] generated using the Perdew-Wang LDA exchange-correlation functional.[24] A self-consistent density was generated with 36 irreducible **k** points, which was then used to calculate energies at 116 **k** points along high symmetry directions to plot the band structure. The kinetic energy cutoff for the plane wave basis was set to 40 Hartrees.

Figure 1 of the important region of the band structure shows the top of the O $2p$ bands, a 2 eV gap to two Nb $4d$ bands which are the highest occupied bands, and another 2 eV gap to the conduction bands. The band gap, direct at the Γ point, is 1.9 eV, somewhat higher than the 1.5 eV reported by Novikov *et al.* (also at the Γ point) using the full potential linear muffin-tin orbital method (FLMTO) with the same structural parameters.[14] LDA calculations often underestimate band gaps, so we conclude that it is most likely the experimental band gap is somewhat larger than 2 eV. Measured optical absorption suggests that the band gap should be around 2 eV,[13] which is consistent with the reported dark reddish color.[13,11]

Projected density of states (DOS) calculations, presented in Fig. 2 were done using the tetrahedron method projecting to atomic spheres with radii of $R(\mathrm{Li})=1.7$ a.u., $R(\mathrm{Nb})=R(\mathrm{O})=2.0$ a.u. These calculations confirm that the upper-

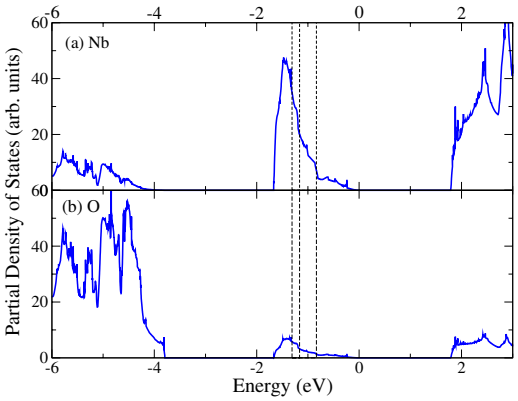

FIG. 2. (Color online) Density of states for Nb and O atoms. For $LiNbO_2$, states are occupied up to energy $E=0$. The dominant states in the valence band for Nb are 4*d* orbitals, and for O they are 2*p* orbitals. Dashed vertical lines are included to indicate the Fermi energy in the rigid band picture for Li_xNbO_2 for concentrations $x=0$ (half-filled band), $x=0.4$, $x=0.8$ from left to right. The last two values of x roughly bracket the concentrations where superconductivity is observed.

most valence bands are largely Nb 4*d* character, with roughly 15% contribution from O 2*p* states, and virtually none from Li states. These projected DOSs are consistent with those calculated by Novikov *et al.*[14] The trigonal crystal field splitting of the Nb 3*d* states results in the d_{z^2} orbital energy centered 4 eV below the other Nb 4*d* states (two e_g doublets, based on $\{xz,yz\}$ and $\{x^2\text{-}y^2,xy\}$). The unit cell contains two symmetry-related Nb layers which result in the presence of two Nb d_{z^2} bands in the band plot. The splitting of the bands along Γ-*M*-*K*-Γ reflects the strength of interaction between layers, as discussed below.

As a result of the large trigonal crystal field splitting, the Nb d_{z^2} state forms a single band, triangular lattice system of the type that is attracting renewed interest. The calculated DOS in Fig. 2 has only a vague resemblance to the nearest neighbor TB model (see, for example, Honercamp[25]) making it evident that longer range hopping must be important. We address this question in detail in Sec. VI.

This general electronic structure, when hole doped, is rather remarkable. It is a *bona fide* representation of a single band system on a triangular lattice, moreover the band is well isolated from other bands. Although single band models are widely used to investigate concepts and to model many-body effects, there are very few actual realizations in real solids. The value of the effective Coulomb on-site repulsion U for Nb^{3+} is not established, but with $W<1.75$ eV it will not require a very large value to lead to correlated behavior. The hole-doped system Li_xNbO_2 provides a unique platform for the detailed comparison of single band models with experimental data, which for thermodynamic properties and for spectroscopic data below 2 eV should involve only the single active band.

IV. ZONE CENTER WAVE FUNCTIONS

We can examine Kohn-Sham wave functions to gain insight into the electronic structure. Shown in Fig. 3 are isosurface plots of the Γ wave functions for the lower and upper valence bands. Both plots reveal the d_{z^2} character of the bands on the Nb atoms, as well as $2p_z$ bonding contributions from the O atoms. For the upper band, the *p* lobes have more weight away from the sandwiched Nb layer, indicating the weight of bonding with O is somewhat decreased. The change in sign between the two Nb layers in Fig. 3(b) indicates the presence of a nodal plane in the Li layer arising from wave function antibonding character (with respect to interlayer coupling).

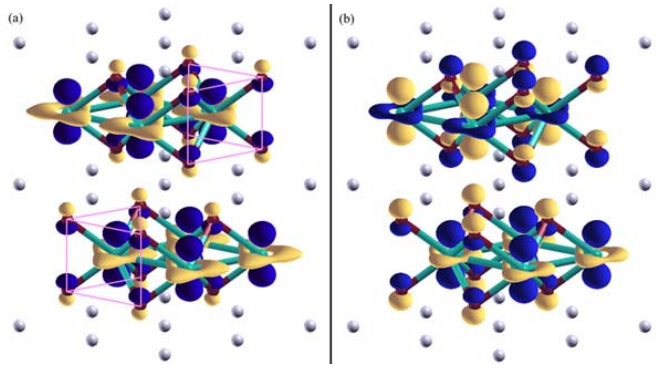

FIG. 3. (Color online) Isosurface plot of the Γ-point wave functions for $LiNbO_2$ for (a) the lower of the pair of valence bands, and (b) the upper valence band, made with XCrysDen (Ref. 26). Both wave functions are generated with the same isosurface value. Nb atoms are turquoise (gray), O atoms are dark red (dark gray), Li are light gray. Yellow and blue (light and dark) indicate opposite signs of the wave function. The z^2 symmetry around the Nb atom is apparent as well as the contribution to the bonding made by the O atoms. Trigonal prisms with O atoms at the corners and Nb atoms in the center have been outlined as a guide to the eye.

The presence of an interesting triangular shape of the wave function around the waist of the Nb atoms is more unexpected, being noticeably larger for the bonding wavefunction. The corners of these triangles do not point toward nearest neighbors, instead they point toward interstitial holes in the Nb layer which are not directly sandwiched between O atoms. This shape reflects either three-center Nb-Nb bonding, which would result in an increased density in this region, or antibonding character of direct Nb-Nb interactions that would decrease the density along the directions connecting Nb atoms. The character and origin of this triangular waist around Nb atoms are clarified in the following section.

V. WANNIER FUNCTION

A single isolated band also provides an unusually clean system for performing the transformation from reciprocal space (bands) to real space (bonds) to look at the character and strength of interatomic interactions from a local viewpoint. The straightforward way of doing this is to generate Wannier functions (WFs) defined by

$$|\mathbf{R}m\rangle = N_{\mathbf{k}}^{-1/2}\sum_{\mathbf{k},n} U_{mn}^{\mathbf{k}} e^{-i\mathbf{k}\cdot\mathbf{R}}|\mathbf{k}n\rangle, \quad (1)$$

where $U^{\mathbf{k}}$ can be any unitary matrix, and $N_{\mathbf{k}}$ is the number of $\mathbf{k}$ points used in the summation. The orthonormal Bloch

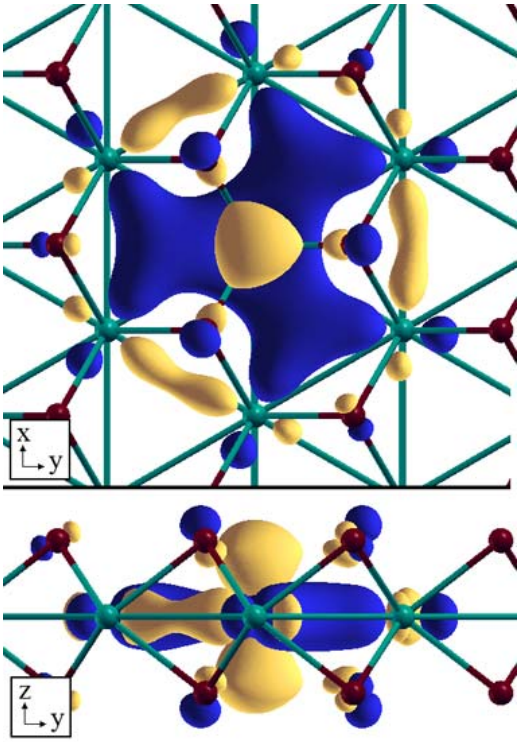

FIG. 4. (Color online) Isosurface plot of the Wannier function for $LiNbO_2$, made with XCrysDen (Ref. 26). Niobium atoms are turquoise (gray), O atoms are dark red (dark gray), Li not pictured. Yellow and blue indicate opposite signs of the WF. The z^2 symmetry around the central atom is apparent, as well as the xy/x^2-y^2 character around nearest neighbors, which maintains the orthogonality of WFs centered on different atoms.

states are denoted by $|\mathbf{k}n\rangle$. If there were only one NbO_2 layer per cell, hence only one band, $U(\mathbf{k})$ would be simply a complex number of unit modulus. Here it is a 2×2 matrix in band space, which gives rise to very modest extra complexity. These WFs display orthonormality $\langle \mathbf{R}m|\mathbf{R}'m'\rangle = \delta_{\mathbf{R},\mathbf{R}'}\delta_{m,m'}$. Once a choice for $U^{\mathbf{k}}$ is made, this approach generates a basis set of identical WFs for each point in the Bravais lattice of the system being studied.

We have chosen the unitary matrix U such that $U = M(M^{\dagger}M)^{-1/2}$ with $M_{mn}=\langle \mathbf{k}n|S_m\rangle$ where $|S_m\rangle$ are a set of atom-centered functions with the desired d_{z^2} symmetry. This technique has been used previously in the study of magnetic ordering in cuprates.[27] Choosing $|S_m\rangle$ as hydrogenic $4d_{z^2}$ orbitals centered on the Nb atoms for the two entangled valence bands gives a pair of identical WFs for each Nb bilayer in the unit cell, based on the Nb d_z^2 symmetry that was also observed in the Γ-point wave function. An $8\times8\times4$ mesh totaling 256 k points was used to generate the WF shown in Fig. 4. Increasing the size of the mesh does not change the visual appearance of the WF.

The WF naturally displays the prominent lobe along the $\pm\hat{z}$ axis that is characteristic of the $3z^2-r^2$ function. It also contains p_σ contributions from the nearest O ions, as well as smaller but still clear $2p$ amplitude on the second neighbor O ions that is approximately p_π. Here p_σ denotes the combination of p_x, p_y, p_z functions oriented toward the reference Nb atom, while p_π is perpendicular. The p_σ lobe nearest the Nb ion has the same sign as the $3z^2-r^2$ lobes along the $\hat{z}$ axis.

The in-plane part of the WF reveals more about the bonding in $LiNbO_2$. The ring structure of the $3z^2-r^2$ function in the x-y plane connects with combinations of xy and x^2-y^2 functions on the three neighboring Nb ions to form a substantial in-plane windmill structure with three paddles, which are oriented between the z projections of the neighboring O ions. A "$3z^2-r^2$" symmetry WF has the full D_{3h} symmetry of the Nb site, which allows a contribution of an appropriate combination of x^2-y^2 and xy atomic orbitals, and the windmill structure reflects the bonding of such functions on neighboring Nb ions. Thus the $4d$ character is not entirely d_{z^2}, which clarifies the threefold symmetric shape around the Nb waist in the $\mathbf{k}=0$ wave function discussed in the preceding section.

In addition, there is a "hotdog" structure of opposite sign connecting pairs of nearest-neighbor Nb ions. Of the two types of Nb-Nb pairs, these hotdogs lie nearest to the first neighbor O ions. Small nearest-Nb "backbonds" in the x-y plane of both the windmill arms and the hotdogs are also evident. As we note below, the WF contains information about the Nb-Nb hopping parameters. The more distant parts of the WF function are a direct reflection of the existence of such longer range interaction.

This Nb $4d_{z^2}$ WF is similar to that for Ta $5d_{z^2}$ in isostructural $TaSe_2$.[28] A difference is that the nearest neighbor O $2p$ orbitals contribute more significantly to the bonding in $LiNbO_2$, giving a larger nearest-neighbor hopping. The d_{z^2} lobes above and below the transition metal appear to be somewhat more pronounced in $TaSe_2$. We also observe changes toward such appearance in this Nb WF as the O layer height (z) is increased, forcing the O atoms closer to the Nb layers and increasing t_1. Given in Fig. 5 is a plot of the *difference* in the magnitudes of the WFs taken for the two different z values of 0.1359 and 0.1263 (O displacements of roughly 0.1 Å). There is an increase in the density of the d_{z^2} lobes above and below the transition metal as well as a tilting of the O orbitals toward the central site, as the Nb-O distance is reduced. Correlating this with the tight binding results from the next section suggests there is an increase in the role the O atoms play in the hopping to nearest neighbors as the Nb-O distance is decreased. The opposite effect occurs when $z=0.1167$; the O orbitals tilt to become oriented more along the z direction, indicating the O atoms are interacting less strongly with Nb.

VI. TIGHT BINDING

The valence bands seen in Fig. 1 are well isolated from bands above and below. These bands contain the superconducting electrons in delithiated Li_xNbO_2, so a simplified tight binding fit using only these bands would be useful in doing studies on simple models. The TB model to fit two bands corresponding to identical Nb d_{z^2}-O p hybridized Wannier functions on the two Nb atoms per cell gives dispersion relations from the roots of

$$0 = \begin{vmatrix} \varepsilon_{\mathbf{k}}^{\parallel} - \varepsilon_{\mathbf{k}} & \varepsilon_{\mathbf{k}}^{\perp} \\ \varepsilon_{\mathbf{k}}^{\perp *} & \varepsilon_{\mathbf{k}}^{\parallel} - \varepsilon_{\mathbf{k}} \end{vmatrix} \Rightarrow \varepsilon_{\mathbf{k}} = \varepsilon_{\mathbf{k}}^{\parallel} \pm |\varepsilon_{\mathbf{k}}^{\perp}|, \tag{2}$$

where $\varepsilon_{\mathbf{k}}^{\parallel}$ arises from the hopping processes within a plane of atoms and $\varepsilon_{\mathbf{k}}^{\perp}$ from hopping between planes. Within the

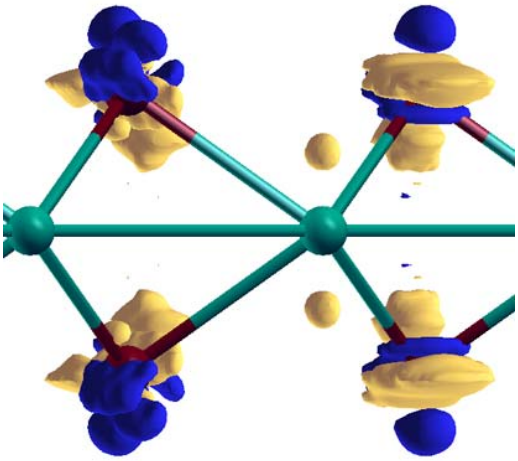

FIG. 5. (Color online) Isosurface plot of the difference $|W_{z=0.1359}(\mathbf{r})|-|W_{z=0.1263}(\mathbf{r})|$, looking along the [010] Cartesian direction. Yellow (light gray) is the positive isosurface and blue (dark gray) is negative, with Nb atoms in turquoise (gray) and O atoms in dark red (dark gray). As the O atoms are moved closer to the Nb layer, there is an increase in density above and below the Nb atom; in addition the contributions from the O-p orbitals appear to tilt more towards the central Nb atom.

plane of the triangular lattice, the nearest neighbor dispersion for the six nearest neighbors is

$$\varepsilon_{\mathbf{k}}^{\parallel} = 2t\left[\cos(k_x a) + 2\cos\left(\frac{1}{2}k_x a\right)\cos\left(\frac{\sqrt{3}}{2}k_y a\right)\right]. \quad (3)$$

We have found that a good fit to the Nb d_{z^2} bands requires several neighbors. Third and fifth neighbors in the plane can be included with this form by noticing odd neighbors just require a larger lattice constant. Second neighbors require a larger lattice constant and a 30° rotation. There are 12 fourth neighbors, which can be treated as two lattices with separate rotations.

First and second neighbors in adjacent layers can be included with terms of the form

$$\varepsilon_{\mathbf{k}}^{\perp} = 2\cos\frac{k_z c}{2}\left\{2t_1^{\perp}\left[\cos\left(\frac{k_x a}{2}\right)e^{ik_y a/2\sqrt{3}} + e^{ik_y a/\sqrt{3}}\right] + 2t_2^{\perp}[\cos(k_x a)e^{-ik_y a/\sqrt{3}} + e^{-i2k_y a/\sqrt{3}}]\right\}. \quad (4)$$

It is worth noting that on the zone surface (where $k_z = \pm\frac{\pi}{c}$), all terms in $\varepsilon_{\mathbf{k}}^{\perp}$, including further neighbors neglected from Eq. (4) are identically zero, resulting in exact degeneracy of the two valence bands at these zone surfaces.

Using the Wannier basis given in the preceding section, the hopping parameters can be *directly calculated* (rather than fit) as matrix elements of the LDA Hamiltonian

$$t_{|R|,m} = \langle \mathbf{R}m|\hat{H}|\mathbf{0}m\rangle, \quad m = 1,2, \quad (5a)$$

$$t_{|R|,m,m'}^{\perp} = \langle \mathbf{R}m'|\hat{H}|\mathbf{0}m\rangle. \quad (5b)$$

Using the definition of the WF along with orthogonality of the eigenfunctions, Eqs. (5) reduce to

$$t_{|R|,m} = N_{\mathbf{k}}^{-1}\sum_{\mathbf{k}n}\varepsilon_{\mathbf{k}n}|U_{mn}^{\mathbf{k}}|^2 e^{i\mathbf{k}\cdot\mathbf{R}}, \quad (6a)$$

$$t_{|R|,m,m'}^{\perp} = N_{\mathbf{k}}^{-1}\sum_{\mathbf{k}n}\varepsilon_{\mathbf{k}n}(U_{m'n}^{\mathbf{k}})^* U_{mn}^{\mathbf{k}} e^{i\mathbf{k}\cdot\mathbf{R}}, \quad (6b)$$

where $\mathbf{R}$ is the difference in centers of the WFs. Deviation of a perfect representation of the bands arises only from approximation of the summation in Eq. (6) or neglect of further neighbors.

The results of the tight-binding calculation are presented in Table I, as calculated from a $12\times12\times6$ Monkhorst-Pack grid of $\mathbf{k}$ points for various values of z, along with values for 2H-$TaSe_2$ as given in Ref. 28. Remarkably, the *second* neighbor hopping integral t_2 is the dominant contribution for $z \leqslant 0.1263$. Also notable is the strong dependence of first and third neighbor hoppings, t_1 and t_3, on the Nb-O distance, which causes t_1 to become largest for z somewhat greater than 0.1263. The other parameters in the table are all relatively independent of the Nb-O distance. The third and beyond interplane hoppings may appear small, but they must be compared keeping in mind that there are twice as many third and fourth interplane neighbors as first and second. Since $t_1^{\perp} \sim 2t_3^{\perp} \sim 2t_4^{\perp}$, even these long distance hoppings are

TABLE I. Tight binding hopping parameters for three values of the O internal structural parameter z. Hopping parameters are reported in meV; bandwidths and band gaps are reported in eV. Distance between Nb and O atoms are reported in angstroms. The largest hopping coefficients are in boldface. Squeezing the O layers closer to the Nb layers (z=0.1359) results in a dramatic increase in t_1, making it larger than t_2, and a large change in t_3 as well. For z=0.1359, the band gap is indirect. The direct gap at Γ is listed followed by the indirect gap in parentheses. See Fig. 7. $t_3^{\perp}$ is slightly refined, to make the splitting at Γ agree with the DFT result better.

z	$d_{\text{Nb-O}}$	Bandwidth	Band gap	t_1	t_2	t_3	t_4	t_5	$t_1^{\perp}$	$t_2^{\perp}$	$t_3^{\perp}$	$t_4^{\perp}$	$t_5^{\perp}$
0.1167	2.178	1.36	1.69	19	**102**	10	−10	6	18	−23	−5	−7	−1
0.1263	2.116	1.67	1.78	64	**100**	33	−13	8	18	−21	−5	−6	−8
0.1359	2.056	2.17	1.89(0.95)	**122**	94	56	−17	9	18	−19	−3	−6	−8
2H-$TaSe_2$		1.9		38	**115**				29	23			

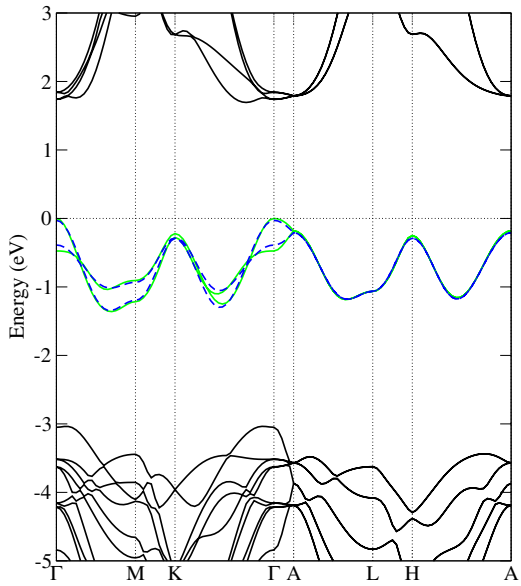

FIG. 6. (Color online) Band structure for O layer position $z=0.1167$, a larger Nb-O layer separation by 0.1 Å compared to the bands in Fig. 1. The bandwidth is 25% smaller, and band gap is less, compared to the experimental structure ($z=0.1263$).

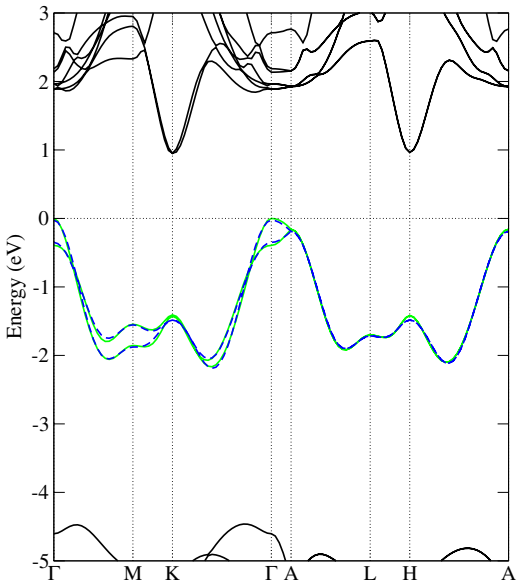

FIG. 7. (Color online) Band structure for O layer position $z=0.1359$, about 0.1 Å closer to the Nb layer than in experiment (Fig. 1). The bandwidth is 15% larger than for the experimental structure, and the peaks at M and K in the valence band are similar to the band structure calculation of $Li_{0.5}NbO_2$ shown by Novikov *et al.* (Ref. 14), suggesting that the underlying electronic structure of Li_xNbO_2 is determined by the position of O layers rather than the Li concentration.

relevant. Indeed, it is not possible to get good agreement in the band splittings at the points Γ, M, K, and the minimum between K and Γ without five interplane hopping parameters (four for $z=0.1167$).

The TB model for $z=0.1167$ is strongly dominated by the second neighbor interactions between the Nb atoms, with other hoppings roughly an order of magnitude smaller. If t_2 were the only hopping parameter present, the system would consist of three disjoint sublattices and thus states would be threefold degenerate (although it would not be obvious on the standard band plot). Including t_1 as a perturbation would couple them weakly and remove degeneracies. In this case, the unit cell of the system could be taken as the second neighbor lattice and the Brillouin zone would be folded back so that the $K(H)$ point in the band plots shown is mapped onto the $\Gamma(A)$ point. The result of this folding back (and the splitting that occurs because of nonzero t_1), is evident in Fig. 6, in that the eigenenergy of the H point is nearly the same as for the A point. The $M(L)$ point is mapped onto itself, and the minimum between $\Gamma(A)$ and $M(L)$ is mapped onto the $K(H)$ point, which results in a band structure that looks very much like a $\sqrt{3}$ larger triangular lattice with only nearest neighbor hopping. Similar dominance of second neighbor hopping has been observed for 2H-$TaSe_2$.[28] Those authors relate their small value for t_1 to phase cancellation of Wannier functions centered at first nearest neighbors, whereas in-phase contributions at second-neighbors give a large t_2 matrix element.

For $z=0.1359$, we find that the nearest neighbor interaction becomes dominant. From Table I and Fig. 5 we see that the increase in hybridization of the O anion p state in $LiNbO_2$ as the Nb-O distance is decreased plays a significant role in first neighbor hopping, while at the same time this hybridization is rather insignificant in second neighbor hopping. This behavior suggests that a significant contribution to the hopping integrals comes from within the Nb planes, perhaps through the hotdog structure noted in the preceeding section. The band structure in this case looks similar to that of $Li_{0.5}NbO_2$, calculated by Novikov *et al.*,[14] especially in the magnitude of the variations around the M and K points, relative to the bandwidth. Their result shows some splitting of the bands occurring at the zone surface (along the lines A-L-H-A), which may arise from the two Nb sites becoming inequivalent due to the removal of one Li atom. If the Nb sites were kept equivalent as the Li is removed, such as in the virtual crystal approximation, then the similarities between the band structures suggest that the main impact on the electronic structure is captured by changing the Fermi energy and allowing the O layers to move closer to the Nb layers, decreasing the Nb-O distance.

Another point of interest we see in Figs. 6 and 7 is a significant change in how the valence band is situated in relation to the O $2p$ bands. Nb $4d$ states in the conduction band around the K point are significantly lowered in energy as the Nb-O distance is decreased so that the band gap becomes indirect and much smaller. This change will have contributions from both a Madelung shift and from changes arising from the altered Nb-O interaction.

VII. ZONE CENTER VIBRATIONAL MODES

We have calculated the $3N-3=21$ optical phonon eigenmodes with $\mathbf{q}=0$. To our knowledge, experimental IR or Raman measurements have not been reported on $LiNbO_2$. However, we believe these results will be useful for comparison

TABLE II. Calculated zone-center phonon frequencies, with LO modes listed where they occur. See the Appendix for detailed descriptions of the atomic motions. All phonons with x-y polarization are doubly degenerate, as required by the hexagonal symmetry. The last six columns show the calculated value of α_i, defined by Eq. (7) for both TO and LO modes.

	Symmetry designation	Phonon frequency (meV)			α for TO			α for LO		
		Polarization	TO	LO	α_{Li}	α_{Nb}	α_O	α_{Li}	α_{Nb}	α_O
1	E_{2g}	x-y	9.4		0	0.38	0.12			
3	B_{2g}	z	18.5		0	0.39	0.11			
4	E_{2u}	x-y	28.8		0.50	0	0.01			
6[a]	E_{1u}	x-y	29.9	33.5	0.48	0.03	0	0.46	0.04	0
8[a]	A_{2u}	z	53.3	70.0	0.47	0.01	0.03	0.43	0.06	0.01
9[b]	E_{2u}	x-y	58.8		0.01	0	0.49			
11	E_{1g}	x-y	59.4		0	0	0.50			
13[a]	E_{1u}	x-y	64.4	71.6	0	0.12	0.38	0.02	0.10	0.38
15	B_{1u}	z	64.5		0.38	0	0.12			
16[b]	E_{2g}	x-y	64.8		0	0.12	0.39			
18[b]	A_{1g}	z	85.4		0	0	0.50			
19[a]	A_{2u}	z	85.5	96.3	0.01	0.14	0.35	0.05	0.09	0.37
20	B_{1u}	z	89.5		0.13	0	0.38			
21	B_{2g}	z	94.8		0	0.11	0.39			

[a]IR active mode.
[b]Raman active mode.

with electron-phonon calculations done on the delithiated Li_xNbO_2, which will be explored in future work. The frequencies are given in Table II. Mode symmetries have been obtained with the use of SMODES, part of the *Isotropy* package of Stokes and Boyer.[29] Masses of the ions used were 6.94 (Li), 92.91 (Nb), and 16.00 (O), all in amu. Also in Table II are given values of the isotope shift α, defined by

$$\alpha_i = -\frac{\partial \ln \omega}{\partial \ln M_i}, \tag{7}$$

where i runs over the different (types of) atoms in the crystal. The derivative was approximated with a centered difference, which, for a harmonic crystal with $\omega \propto M^{-1/2}$, introduces errors of order $(\frac{\delta M}{M})^2$. Using $\delta M = 1$ amu, this amounts to an error of about 2% for Li, and less for heavier elements. One would expect $\Sigma_i \alpha_i = \frac{1}{2}$ for a harmonic mode.

The dielectric tensor for a hexagonal system such as this will be diagonal with two distinct elements. For frequencies much higher than phonon frequencies but well below the gap, the static dielectric constants, calculated without ionic contributions, are found to be $\epsilon_\infty^x = 10.3$ and $\epsilon_\infty^z = 3.78$. One can then use the generalized Lyddane-Sachs-Teller relation, $\epsilon_0^\alpha = \epsilon_\infty^\alpha \Pi_m (\omega_{LO,m}^\alpha / \omega_{TO,m}^\alpha)^2$ (where α runs over the Cartesian directions, and the product is taken over all IR active modes with polarization in that direction) to include the ionic contribution for the low frequency dielectric constant. Doing so, we find for $LiNbO_2$ that $\epsilon_0^x = 15.9$ and $\epsilon_0^z = 8.27$. It is typical for LDA calculations to overestimate somewhat the dielectric constants, presumably due to the band gap being underestimated.

The eigenmodes fall into groups which are easily distinguishable by frequency. In the following discussion we include degeneracy in the numbering of modes. The first group, modes 1-3, are low frequency modes involving displacements of massive Nb-O layers against each other, with Li layers remaining fixed. The second group, modes 4–7, involve the lighter Li layers, and lie around 29 meV. The third group, modes 8–17 in the 53–65 meV range, involve motions where layers of atoms slide in the x-y plane against adjacent layers of atoms, or groups of layers bounce against each other in the z direction. The last group of modes at 85–95 meV involves layers nearby each other bouncing against each other in the z direction. A more detailed discussion of the individual modes is given in the Appendix.

VIII. EFFECTIVE CHARGES

Born effective charge calculations have been carried out as described by Gonze and Lee.[31] The calculation was done using a plane wave cutoff of 60 Ha and 200 **k** points in the Brillouin zone to give effective charge tensors Z^* for each atom which are diagonal, and obey $Z_{xx}^* = Z_{yy}^*$, as required by symmetry for a hexagonal crystal. Results are given in Table III for the relaxed atomic structure. The effective charges of $NaCoO_2$ have been included in this table to illustrate the strong similarity between these two systems, which are similarly layered transition metal oxides but otherwise their electronic structures are quite different.

The effective charges of $LiNbO_2$ are rather different than those reported by Veiten and Ghosez[3] for $LiNbO_3$. There are structural and chemical differences responsible for this; the

TABLE III. Calculated Born effective charges for $LiNbO_2$, compared with those calculated for $NaCoO_2$ by Li *et al.* (Ref. 30). Note the disparity in the effective charges for the alkali metals and the transition metal in the z-direction. For O however, Z^* is not far from isotropic.

	$LiNbO_2$			$NaCoO_2$		
	Li	Nb	O	Na	Co	O
Z^*_{xx}	1.10	2.26	−1.68	0.87	2.49	−1.68
Z^*_{zz}	1.69	1.31	−1.50	1.37	0.87	−1.12
Z^{Formal}	+1	+3	−2	+1	+3	−2

structure of $LiNbO_3$ has Nb coordinated in a distorted octahedral environment and thus has low symmetry. Perhaps more importantly, the formal charges of Nb are very different: Nb^{3+} in $LiNbO_2$, but Nb^{5+} in $LiNbO_3$, leaving the formal electronic configuration of Nb in $LiNbO_3$ as d^0. The effective charges of such ions are known to sometimes be rather large, as is the case in $LiNbO_3$.

Z^*_{xx}(Li) is close to the formal charge of Li indicating ionic type response for in-plane motion. In fact, all ions have effective charge closer to the formal value for in-plane displacement than for $\hat{z}$ displacement. The charge tensor for Li shows similar anisotropy to that of Li in LiBC,[32] where it was inferred that Li is involved chemically in coupling between B-C layers. Similarly here, it can be expected that Li has chemical involvement in interlayer coupling between the electron rich Nb-O layers more so than Na does in Na_xCoO_2. This involvement is not strong enough to inhibit deintercalation, however.

The smaller than formal charges for Nb indicates substantial covalent character to the bonding, which is especially strong in the $\hat{z}$ direction. This charge renormalization may be related to the strong change in band structure due to change of the distance between the Nb and O layers, discussed in earlier sections.

IX. SUMMARY

In this work we have examined the electronic structure, the Wannier functions of the valence bands and their tight-binding parametrization, and several vibrational properties of the quasi-two-dimensional material $LiNbO_2$. These basic properties are important in providing the basis for understanding the behavior of the system when it is hole doped by deintercalation of Li.

Li_xNbO_2 seems to be a candidate for an insulator-to-superconductor transition, as it undergoes an insulator-to-metal transition and becomes superconducting, but doping studies are not systematic enough yet to shed light on this possibility. Phase space considerations in two-dimensional materials lead to superconductivity that is independent of doping level, at least when the Fermi level is not far from a band edge.[19] This property supports the possibility of an insulator-superconductor transition with doping, i.e., as soon as it becomes metallic it is superconducting.

The Wannier function, centered on and based on the occupied Nb d_{z^2} orbital, illustrates graphically not only how Nb bonds with neighboring O ions, but also that it couples with oxygens in adjoining layers. Inspection of the **k**-space wave function suggests there are direct Nb-Nb interactions within the d_{z^2} band as well as indirect coupling through O ions.

A tight binding representation of the band, obtained by direct calculation (rather than fitting) using the Wannier function, reveals that several neighbors both in-plane and interplane are necessary to reproduce the dispersion. To model the interlayer interaction precisely requires four to five interlayer hopping parameters. For the experimental structure intralayer hopping is dominated by second neighbor hopping, but the strength of both first and third neighbor hopping is strongly modulated by varying the Nb-O distance. This electron-lattice coupling provides one possibility for the superconducting pairing mechanism in Li_xNbO_2.

Comparison with previous calculations of the band structure of $Li_{0.5}NbO_2$ suggests that the electronic structure of Li_xNbO_2 can be modeled in virtual crystal fashion, or perhaps even in rigid band fashion if that is convenient. The Nb d_{z^2} band is remarkably well isolated from neighboring bands by Madelung shifts and crystal field splitting. We suspect that the overriding importance of this system will result from its unique standing as a single band, triangular lattice system for which sophisticated studies on simple models may be directly comparable to experimental data.

Note added in proof: Recently, a new work by Liu *et al.*[33] has come to our attention. This article provides experimental evidence that the superconductivity of Li_xNbO_2 with $x=0.68$ is conventional s-wave superconductivity, which supports our supposition that pairing is phonon-driven.

ACKNOWLEDGMENTS

The authors have benefited from communication with K. E. Andersen and A. Simon. Some of the calculations of $LiNbO_2$ wave functions used to compute tight binding parameters were done on machines at Lawrence Livermore National Laboratory. This work was supported by National Science Foundation Grant No. DMR-0421810.

APPENDIX: PHONON MODE DESCRIPTIONS

The following is a descriptive list of the atomic motions for each mode given in Table II, grouped by their spectroscopic activity. Degeneracy is included in the numbering of modes.

Silent modes

Modes 1–2: NbO_2 layers slide against each other in the x-y plane.

Mode 3: NbO_2 layers bounce against each other in the z direction.

Modes 4–5: LiO_2 layers slide against each other in the x-y direction. Li displacements are roughly an order of magnitude larger than O displacements, which results in the mass of the O atoms having very little effect on the frequency of this mode.

Modes 11–12: Adjacent O layers slide against each other, with Li and Nb layers remaining stationary.

Mode 15: LiO_2 layers bounce against each other in the z direction. This is the one high frequency mode whose isotope shift α gets its major contribution from the Li atoms.

Mode 20: Out-of-phase Li layers beat against adjacent O layers in the z direction.

Mode 21: Out-of-phase Nb layers beat against adjacent O layers in the z direction.

IR active modes

Modes 6–7: In-phase Li layers sliding against NbO_2 layers. The main contribution to α comes from the light Li atoms, with the heavy NbO_2 layers making very little contribution. This mode is also IR active, with a small LO-TO splitting $\Delta\omega=\omega_{LO}-\omega_{TO}=3.6$ meV.

Mode 8: The TO mode consists of Li layers bouncing against NbO_2 layers in the z direction, and can be thought of as the "z-polarized version" of modes 6 and 7. When the macroscopic electric field is included, the O displacements change sign and the mode becomes Li-O layers bouncing against Nb layers. $\Delta\omega=16.7$ meV.

Modes 13–14: Li and Nb are in synchronized sliding against O layers. The metal layers are all in phase with each other, and out of phase with the O layers. This mode is IR active, with $\Delta\omega=7.2$ meV.

Mode 19: The transverse mode consists of LiO_2 layers beating against Nb layers in the z direction. The Li-O layers are all in phase. This mode is IR active, and once the macroscopic electric field is included, this mode can be characterized as having Nb layers bounce against adjacent O layers, where the Nb layers are out of phase. $\Delta\omega=10.8$ meV.

Raman active modes

Modes 9–10: Out-of-phase Li layers slide in the x-y direction against adjacent O layers. The rest of the phonon modes from here on have the contribution to their isotope shift α dominated by O.

Modes 16–17: Out-of-phase Nb layers slide against adjacent O layers in the x-y plane.

Mode 18: The O layers beat against each other in the z direction. This fully symmetric Raman active mode is of particular interest, as it corresponds to the variation of the internal structural parameter z. This mode has a significant impact on the electronic structure as discussed in the preceding sections, so we suspect that it may have particularly strong electron-phonon coupling in hole-doped Li_xNbO_2.

Clarifying comments

The z-polarized A_{2u} IR active modes 8 and 19 have their eigenvectors affected by the inclusion of the macroscopic electric field. Without the electric field, the eigenmodes can be described as one where Nb layers bounce against Li-O units and one where Li layers bounce against Nb-O units. The application of the electric field causes these vectors to mix, and the descriptions change so that the latter one is replaced by a mode where Li and Nb bounce against O layers. The distinction between these two modes is the relative sign for Li and Nb displacements (negative for the former, positive for the latter). It is not unusual to have modes mix to give different LO modes, as the nonanalytic part of the dynamical matrix which incorporates the electric field can have eigenvectors differing from the analytic part of the dynamical matrix, resulting in a mixing of modes of the same symmetry. This is discussed in some detail by Gonze and Lee.[31] This complicates the association of LO modes with their corresponding TO mode, so we have chosen to pair the LO and TO modes such that $\omega_{LO}>\omega_{TO}$.

[1] M. J. Geselbract, T. J. Richardson, and A. M. Stacy, Nature (London) **345**, 324 (1990).

[2] J. Köhler, C. Svensson, and A. Simon, Angew. Chem., Int. Ed. Engl. **31**, 1437 (1992).

[3] M. Veithen and P. Ghosez, Phys. Rev. B **65**, 214302 (2002).

[4] V. A. Gasparov, G. K. Strukova, and S. S. Khasanov, JETP Lett. **60**, 440 (1994).

[5] G. K. Strukova, V. V. Kedrov, V. N. Zverev, S. S. Khassanov, I. M. Ovchinnikov, I. E. Batov, and V. A. Gasparov, Physica C **291**, 207 (1997).

[6] V. A. Gasparov, S. N. Ermolov, G. K. Strukova, N. S. Sidorov, S. S. Khassanov, H.-S. Wang, M. Schneider, E. Glaser, and W. Richter, Phys. Rev. B **63**, 174512 (2001).

[7] Y. Takano, S. Takayanagi, S. Ogawa, T. Yamadaya, and N. Môri, Solid State Commun. **103**, 215 (1997).

[8] M. Kato, A. Inoue, I. Nagai, M. Kakihana, A. W. Sleight, and Y. Koike, Physica C **388-389**, 445 (2003).

[9] J. E. L. Waldron, M. A. Green, and D. A. Neumann, J. Phys. Chem. Solids **65**, 79 (2004).

[10] E. N. Andersen, T. Klimczuk, V. L. Miller, H. W. Zandbergen, and R. J. Cava, Phys. Rev. B **72**, 033413 (2005).

[11] G. Meyer and R. Hoppe, Angew. Chem., Int. Ed. Engl. 13 (1974).

[12] J. K. Burdett and T. Hughbanks, Inorg. Chem. **24**, 1741 (1985).

[13] M. J. Geselbracht, A. M. Stacy, A. R. Garcia, B. G. Silbernagel, and G. H. Kwei, J. Phys. Chem. **97**, 7102 (1993).

[14] D. L. Novikov, V. A. Gubanov, V. G. Zubkov, and A. J. Freeman, Phys. Rev. B **49**, 15830 (1994).

[15] E. G. Moshopoulou, P. Bordet, and J. J. Capponi, Phys. Rev. B **59**, 9590 (1999).

[16] N. Kumada, S. Watauchi, I. Tanaka, and N. Kinomura, Mater. Res. Bull. **35**, 1743 (2000).

[17] S. Yamanaka, H. Kawaji, K. Hotehama, and M. Ohashi, Adv. Mater. (Weinheim, Ger.) **8**, 771 (1996).

[18] A. Cros, A. Cantarero, D. Beltrán-Porter, J. Oró-Solé, and A. Fuertes, Phys. Rev. B **67**, 104502 (2003).

[19] W. E. Pickett, J. M. An, H. Rosner, and S. Y. Savrasov, Physica C **387**, 117 (2003).

[20] A. F. McDowell, D. M. Snyderman, M. S. Conradi, B. G. Silbernagel, and A. M. Stacy, Phys. Rev. B **50**, 15764 (1994).

[21] A. P. Tyutyunnik, D. G. K. V. G. Zubkov, V. A. Pereliaev, and A.

E. Kar'kin, Eur. J. Solid State Inorg. Chem. **33**, 53 (1996).
[22] X. Gonze *et al.*, Comput. Mater. Sci. **25**, 478 (2002), the ABINIT code is a common project of the Université Catholique de Louvain, Corning, Incorporated, and other contributors (URL http://www.abinit.org).
[23] N. Troullier and J. L. Martins, Phys. Rev. B **43**, 1993 (1991).
[24] J. P. Perdew and Y. Wang, Phys. Rev. B **45**, 13244 (1992).
[25] C. Honerkamp, Phys. Rev. B **68**, 104510 (2003).
[26] A. Kokalj, J. Mol. Graphics Modell. **17**, 176 (1999), code available from http://www.xcrysden.org/
[27] W. Ku, H. Rosner, W. E. Pickett, and R. T. Scalettar, Phys. Rev. Lett. **89**, 167204 (2002).
[28] R. L. Barnett, A. Polkovnikov, E. Demler, W.-G. Yin, and W. Ku, Phys. Rev. Lett. **96**, 026406 (2005).
[29] H. T. Stokes and L. L. Boyer, SMODES, 2002, www.physics.byu.edu/~stokesh/isotropy.html
[30] Z. Li, J. Yang, J. G. Hou, and Q. Zhu, Phys. Rev. B **70**, 144518 (2004).
[31] X. Gonze and C. Lee, Phys. Rev. B **55**, 10355 (1997).
[32] K.-W. Lee and W. E. Pickett, Phys. Rev. B **68**, 085308 (2003).
[33] G. T. Liu, J. L. Luo, Z. Li, Y. Q. Guo, N. L. Wang, D. Jin, and T. Xiang, Phys. Rev. B **74**, 012504 (2006).